Preprint: Accepted to the International Conference on Robotics and Automation (ICRA) 2025

A Tugging Controller that Maximizes Lateral Resistive Force by Mounding Sandy Terrain

Deaho Moon[1], Chris Huang[2], Justin Page[3], and Hannah S. Stuart[1*]

***Abstract*— Sandy environments present challenges for robotic space rovers and systems due to reduced traction, limiting mobility and tugging force. This paper presents an anchoring method that utilizes a winching system to create a sand mound in front of a mobile agent dragged through the media. The proposed controller is designed to consistently achieve real-time capture of close-to-maximal lateral sand mound resistive force, even when applied to varied uneven terrains, like holes or waves. Notably, tugging is non-reversible, so suitable peaks should be captured before breakdown and without necessarily knowing the global optimum *a priori*. The controller logic tracks both tugging force and agent pitch gradients to detect terrain conditions and peak force trends. Results show that the controller captures an average 92% of the maximum forces, within the previously winched workspace tested, across three different granular media with four varying structured terrain features. The controller achieves higher resistive force peaks on terrains with geometric features, as opposed to flat sand. We conclude that sand mounding through tugging is a viable means to generate robotic resistive forces for unknown sandy terrains, a simple yet effective anchoring mechanism.**

I. Introduction

Mobile robots for planetary exploration missions face challenges due to low traction and unknown geometric features of the sandy environment. Orbiters with high-resolution cameras, such as HiRISE on Mars Reconnaissance Orbiter, provide surface images with a resolution of approximately 90 cm for object detection [1]. Data from previous landers and rovers show that regolith properties, such as density and grain size – that cannot yet be detected by orbiters – differ by site and impact rover performance [2], [3]. Mobile robotic systems should reliably overcome such uncertainties when they operate at sandy sites.

Tethered mobile robotic team concepts provide one avenue to generate terrain resilience [4]. The DuAxel rover, for example, demonstrates how one agent anchors while the other explores down cliffs or craters while connected by a tether to each other for returning [5]. Different systems utilize fixed anchor base(s) on soil coupled with a mobile rover [6]–[8]. Page et al. introduced a unique robotic payload delivery method on sandy terrain, exploiting the capstan effect by wrapping connecting tethers around on-site objects [9]. This system requires rocky topological features on-site to hold anchoring forces, which may not always be present.

For sandy terrains without rocks available, researchers have developed approaches based on Granular Resistive Force Theory (RFT) to better understand robotic locomotion and anchoring performance; their results established analyses of the resistive forces of an immersed rigid body in sand to improve underground burrowing and tugging [10]–[12]. In particular, Tae et al. and Fernandez et al. demonstrate novel robotic payload delivery methods on granular media by self-burrowing a legged robot and dynamic tail impacts and plowing, respectively [12], [13].

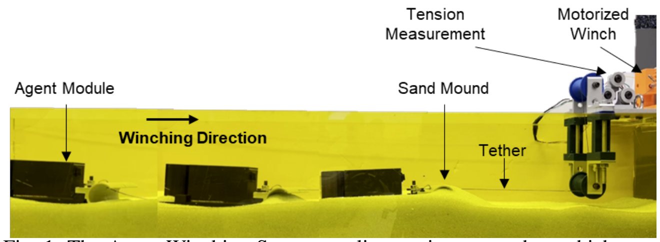

Fig. 1: The Agent Winching System applies tension to a tether, which tugs the Agent Module through the granular media, resulting in a sand mound.

In this paper, we study a robotic agent anchoring method for granular surfaces using sand mound creation alone – without legged burrowing or tail impacts – achieved by an agent winching system that simply tugs a passive anchoring agent. Fig. 1 demonstrates how our approach anchors an agent by creating a sand mound instead of in-depth penetration through the soil used by other robotic anchoring methods. The idea is that the mounding agent – a simple and lightweight anchor – can be projected far from the payload winch, then tugged towards the payload to achieve peak lateral strength for use in forceful manipulation, achieved with modest hardware. The concept and testing of "launchable lunar anchors" across different anchor shapes are described in [14]. This architecture could be useful in the National Aeronautics and Space Administration (NASA) Jet Propulsion Lab's Lunar Crater Radio Telescope (LCRT) project, which utilizes agent anchors on the rim of a lunar crater [15]. However, prior work does not yet address tugging controller design and focuses on anchor ground penetration rather than primarily leveraging mounding forces.

We explore a set of sensor and controller configurations to estimate maximal tugging forces for this type of system. For practical use, it should be robust to uncertain terrain features like existing mounds and holes and unknown granular media properties. Instead of attempting to perform visual classification of terrain on the distal agent using a camera, which is difficult in the harsh lighting of some alien environments [16], we propose to use only agent pitch and tension sensors alone. To do so, we leverage the model developed by Percier et al., which uniquely estimates effective Coulomb Friction

[1] Dept. of Mech. Eng., U of California Berkeley, Berkeley, CA, USA.
[2] Dept. of Mech. Eng., U of Texas, Austin, Austin, TX, USA.
[3] NASA Jet Propulsion Laboratory, Pasadena, CA, USA.
*Corresponding author hstuart@berkeley.edu
This paper has a supplemental video associated with it.

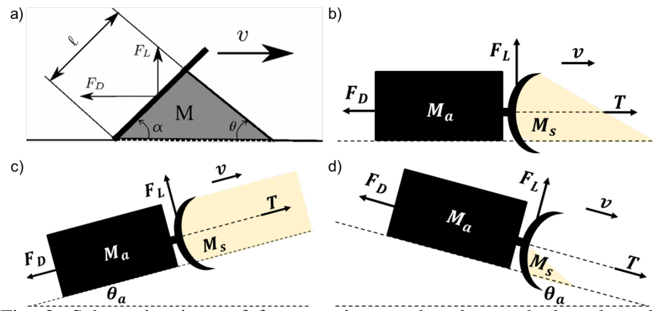

Fig. 2: Schematic views of forces acting on the plow and plowed sand mound geometry: (a) the inclined plow (from [17]), the agent on (b) flat terrain (c) ascending slope and (d) descending slope.

Fig. 3: Mass of plowed sand mound ($M(\theta_a)$) by (a) flat terrain ($M_{s,f}$), (b) ascending slope ($M(\theta_a > 2°)$) and (c) descending slope ($M(\theta_a < -2°)$)

based on the lift and drag force analysis on an inclined plow generating a mound in granular media [17].

A. Overview

Section II introduces the agent tugging force model. Section III then presents the implementation of the agent winching system, with an IMU and tension sensor, and the Force-Pitch Gradient Tracking (FPGT) controller logic. Section IV describes the experimental setup and methods for testing controller efficacy with four different terrain features on three different granular media. In Sections V and VI, we present our experiment results and discuss the controller's ability to capture maximal tugging force within the tested workspace. We provide conclusions in Section VII.

II. Anchor Force Modelling

Fig. 2a shows a schematic view of drag and lift forces acting on an inclined plow and the geometry of the sand mound created by plowing. Percier et al. derived a linear relationship between the drag force F_D, the lift force F_L on the plow, and the weight of sand mound Mg by modeling the mound mass as a solid block sliding over a flat granular bed using the Coulomb friction as in

$$F_D = \mu_{eff}(F_L + Mg) \tag{1}$$

where μ_{eff} is a single effective friction coefficient [17].

By exploiting Eq. (1), our agent tugging force model on flat terrain can be derived as:

$$F_D = \mu_a M_a g + \mu_s (F_L + M_s g) \tag{2}$$
$$T = -F_D \tag{3}$$

with the addition of the mass of the agent and plowed sand mound, M_a and M_s, and the friction coefficients, μ_a and μ_s, between the agent and the sand mound block to the granular bed, respectively, as illustrated in Fig. 2b. In Eq. (3), T represents the agent tugging force or cable tension, the reaction force to F_D, which is equivalent to the agent anchoring force by assuming a constant winching velocity, v. We assume tugging direction remains parallel to v.[1]

As the agent displaces across and overcomes unknown terrain features, the model should account for various agent pitch conditions – tugging up or down – illustrated in Fig. 2c-d. Experimentally, we observed that the agent plows more mass when climbing uphill and loses sand when descending downhill compared to flat terrain, as shown in Fig. 3. Intuitively, this is because the maximum incline angle of the granular media in the Newtonian frame, or the angle of repose, remains constant; while the anchoring agent angle changes, it can scoop up more or less sand before the sand slides out. Hence, M_s is a function of the agent pitch, θ_a, which increases or decreases with an unknown amount of sand change, ΔM_s, from the saturated sand mound mass on flat terrain, $M_{s,f}$. Likewise, F_L and F_D become functions of θ_a with normal and parallel force decomposition by incorporating the inclined plane analysis. The complete agent tugging force model is

$$M_s(\theta_a) = M_{s,f} + \Delta M \sin\theta_a \tag{4}$$
$$F_L = F_{L,f} + M_s(\theta_a) g \cos\theta_a \tag{5}$$

$$\begin{aligned} F_D = {} & M_a g(\sin\theta_a + \mu_a \cos\theta_a) \\ & + M_s(\theta_a) g (\sin\theta_a + \mu_s \cos\theta_a) \\ & + \mu_s F_L \end{aligned} \tag{6}$$

where $F_{L,f}$ is the lift force on flat terrain; this constant depends on the plow geometry and granular media properties and assumes the agent has reached maximum M_s.

The controller should respond robustly to the uncertain constants and variables of a new environment, such as friction coefficients and the amount of sand change in Eq. (6). Because F_D is highly dependent on θ_a, this model supports the use of agent pitch measurement to exploit its ascending state and avoid descending. Even in the flat state ($\theta_a \approx 0°$), small changes in θ_a due to unevenness and mounding can generate substantial fluctuations in F_D. Note that F_D may depend on winching speed and dynamic effects of the granular media; in this work we assume quasistatic motion.

III. System and Controller Implementation

A. Agent Winching System Hardware

The two main hardware components of the agent winching system are an agent module and a winch module. Fig. 4a showcases the agent module (127 mm x 167 mm), equipped with a 3D-printed plow blade, a fixed C-shaped design (18 mm inner radius, 2 mm thick)[2] for consistency, at the front for sand mound creation. The agent module carries 600 grams of disc weights at the rear to balance the moment induced by resistive forces acting on the plow. The Adafruit BNO055 IMU sensor samples the agent pitch, which is then

[1] We do not account for the tugging angle by assuming the anchoring agent is far from the winch module so small vertical displacements are negligible and the cable runs parallel to the average terrain surface.

[2] This shape resembles a bulldozer blade and is scaled in size to achieve tugging forces of less than 100 N for the current experiments. The details of the blade are otherwise arbitrary; other anchors could provide higher forces.

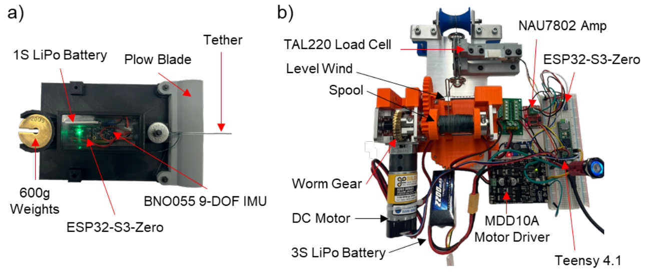

Fig. 4: (a) and (b) show the implementation details for the Agent Module and Winch Module with Tri-wheel Tension Measurement unit, respectively.

transmitted to the winch module over ESP-NOW wireless protocol by the ESP32-S3-Zero transmitter.

The winch module is driven by a 12V 5.2:1 planetary gear DC motor with 28 CPR encoder and the Cyclotron MDD10A DC motor driver, as shown in Fig. 4b. A 28:1 worm gear drive is employed to prevent the winch from back-driving under high tugging forces. A spectra braided fishing line tether is managed by a 2 cm diameter spool and a level wind system similar to a fishing reel attached to the worm gear drive shaft. The cable tension is measured by a TAL220 load cell implemented in the Tri-Wheel design. A SparkFun NAU7802 amplifier then amplifies the load cell reading. The ESP32-S3-Zero receiver receives the agent pitch via ESP-NOW and sends it over I2C to Teensy 4.1, the system's primary controller for sensor data processing and execution of the FPGT controller logic. To estimate quasistatic winching, we set the agent's linear velocity to be 2 mm/s with 2 rpm winching speed.

B. Definition of User-tuned Controller Parameters

Table I describes the tuned parameters for the FPGT controller, with values used in this work. The saturation distance, d_s is selected to avoid capturing a local maximum anchoring force in the initial low tension range. We approximate d_s based on the volume of the expected fully saturated sand mound (on flat terrain) with an angle of repose, θ_{repose}, and the initially submerged plow cross-sectional area, as demonstrated in Fig. 5. Pitch threshold, θ_{th}, represents an interval around $\theta_a = 0°$ used to classify agent pitch. The pitches above the upper threshold, within the upper and lower boundary, and below the lower threshold are interpreted as ascending, flat, and descending terrain, respectively.

Real-time measurements of agent pitch θ_A and tension T are both smoothed to reduce sensitivity to small amplitude dynamic variations due to granular media interactions or sensor resolution. This is especially important when utilizing the gradients of these variables in controller design. We use the Exponential Weighted Average Filtering factors or weights, α, whose magnitude ($0 \leq \alpha \leq 1$) sets the degree of data filtering or smoothing in real-time, as in Eq. (7):

$$y[k] = \alpha x[k] + (1-\alpha)y[k-1] \tag{7}$$

where $y[k]$ is the filtered output, $x[k]$ is the current input, and $y[k-1]$ is the filtered output at the previous time step. The α weight close to 1 delivers more weight to recent incoming data and less smoothing. We additionally introduce a tension attenuation term, which we use to monitor the overall tension trend along winching displacement with a low α to purposefully monitor persistent overall trends in tension. The three α values may need to be tuned depending on system, functional objectives, and granular media properties.

Parameters	Definitions	Tuned Values
d_s	Saturation Distance	20 cm
θ_{th}	Pitch Threshold	$\pm 2°$
$\theta_{A_{\alpha=smooth}}$	Pitch Smoothing Factor	$\alpha = 0.005$
$T_{\alpha=smooth}$	Force Smoothing Factor	$\alpha = 0.01$
$T_{\alpha=attenuated}$	Force Attenuation Factor	$\alpha = 0.001$

TABLE I: Force-Pitch Gradient Tracking Controller Parameters

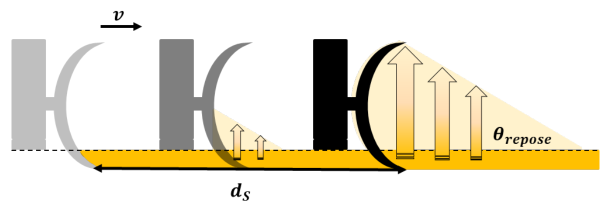

Fig. 5: Saturation Distance (d_s) Demonstration

C. Controller Logic Design

Fig. 6a shows the FPGT controller logic flowchart developed based on the insights from our agent tugging force model, parameter setup, and data collection. Because the controller aims to capture a maximal resistive force, the logic's fundamental idea is a real-time gradient ascent-mannered peak force search with agent tugging force and pitch gradients monitoring. The controller keeps winching to capture a higher force if the measured force is constant or increasing with a constant velocity in every state except for the terminal state, State 4 - Stop, where all the logic condition sequences are satisfied. The controller has five states based on a state machine structure: 0 Sand Mound Creation, 1 Flat and Descending, 2 Flat Test, 3 Ascending, and 4 Stop.

The program initializes to State 0, in which it performs a set winching distance up to d_s. The motor continues winching in State 1 until a number of conditions are met. If the agent is on a flat surface ($-2° \leq \theta_a \leq 2°$), the controller tracks the tugging force gradient, $\nabla T = T(k) - T(k-1)$, to look for a peak force that occurs when the tension gradient becomes $\nabla T < 0$, or the force is decreasing and thus a peak is detected. The controller then searches for a decrease in the smoothed force gradient, $\nabla T_{\alpha=0.01} < 0$, to confirm the peak is persistent. If smoothed peak force is detected, the controller looks at the attenuated tugging force gradient, $\nabla T_{\alpha=0.001}$, to see the overall force trend developed by accumulated data points. If $\nabla T_{\alpha=0.001} < 0$, this indicates the sand resistive force has entered a plateau, or a steady state. Therefore, the last condition to meet in State 1 is that the smoothed agent pitch gradient $\nabla \theta_{A_{\alpha=0.005}} \geq 0$. If true, this series of conditions indicates a sustained flat region, and then the controller enters state 2. When transitioning from State 1 to State 2, the observed peak tugging force is recorded for

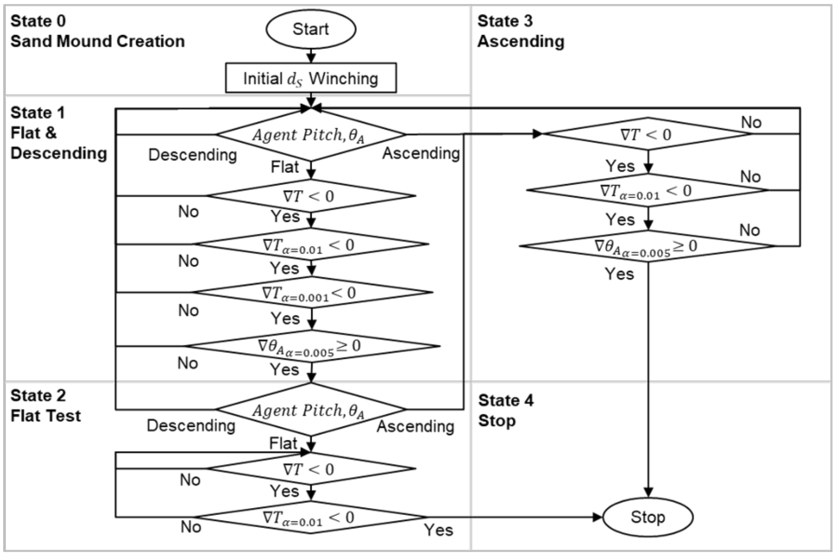

(a) FPGT Controller Logic Flowchart

(b) Granular Media Testbeds (top to bottom): MARS90, Glass Beads, and Beach Volleyball Court.

Fig. 6: State machine logic diagram (a) and testbed media (b) used in experiments.

comparison to the force when transitioning to State 4. State 2 is designed to stop winching – by transitioning to State 4 – at the next detected peak. If the agent remains flat during State 2, the controller detects the next peak force using the $\nabla T < 0$ and $\nabla T_{\alpha=0.01} < 0$ conditions. If the agent goes into ascent or descent, the state changes accordingly.

When the agent is ascending in State 1 or State 2, the controller transitions to State 3. As the agent climbs uphill, the tugging force will decrease near the summit or plateau, where the plow starts losing sand, and the controller should stop before this occurs. Therefore, the controller conservatively aims to capture the first peak detected in the state. This state uses the same tension gradient conditions as State 2 to transition to State 4; an addition pitch gradient check ensure ascent as $\nabla \theta_{A_{\alpha=0.005}} \geq 0$. If any of the conditions is not satisfied, the controller returns to State 1.

IV. Experimental Methods

We test the effectiveness of the FPGT controller across three granular media and four pre-defined terrain features.

A. Granular Media Testbeds

The granular media are selected as MARS90, glass bead, and beach volleyball sand, as shown in Fig. 6b. The MARS90 bed, a fine Mars regolith simulant, has a density of 1.46 g/cm^3 with 0.2 mm grain size, and its volume is 180 cm x 90 cm x 20 cm [18]. The glass bead bed has a 1.43 g/cm^3 density with a mixture of 1 - 2 mm diameter grains. The bed volume is 100 cm x 18 cm x 30 cm [19]. The beach volleyball sand bed is an outdoor environment at UC Berkeley Beach Volleyball Sand Court at Clark Kerr Campus with a mixture of five loosely compacted sand grains whose specifications are set by Fédération Internationale de Volleyball [20]. The measured density of the sand is 1.75 g/cm^3.

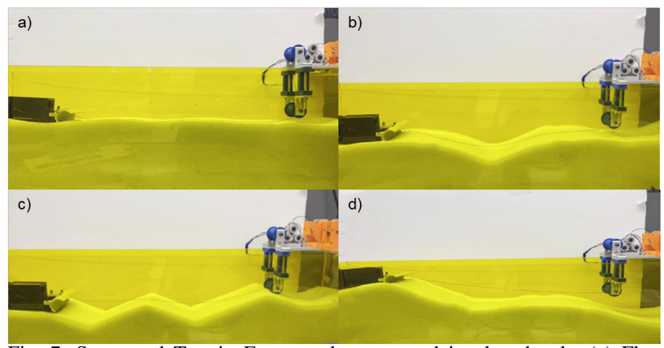

Fig. 7: Structured Terrain Features demonstrated in glass beads: (a) Flat, (b) Hole, (c) Sine, and (d) Downhill.

B. Structured Terrain Features

Fig. 7 shows each granular bed's four structured terrain features. The other terrain features, except for the flat terrain, are designed to simulate the controller logic's worst-case scenarios. Thus, flat terrain will be considered as a reference case for comparison. The hole in Fig. 7b is located at the end of d_s, placed 20 cm in front of the agent. By doing so, the initially created sand mound mass in State 0 will be dumped into the hole, and the controller will start with a lower tugging force than flat terrain. Fig. 7c is a sine wave-shaped terrain where the agent experiences exaggerated repeated unevenness. Fig. 7d shows a downhill slope the agent descends along to examine how the controller behaves with sustained downhill travel.

For flat terrain, a granular bed is leveled by a leveler before each trial to remove any uneven features. The hole and sine features are constructed by making features with scooping out about 3 L of sand on flat terrain. The downhill feature is produced by pouring sand multiple times at a specific location to generate a slope angle by each granular medium's own θ_{repose}. Likewise, to maintain consistency in data collection, the unwanted features created from previous trials are removed and smoothed by the tools.

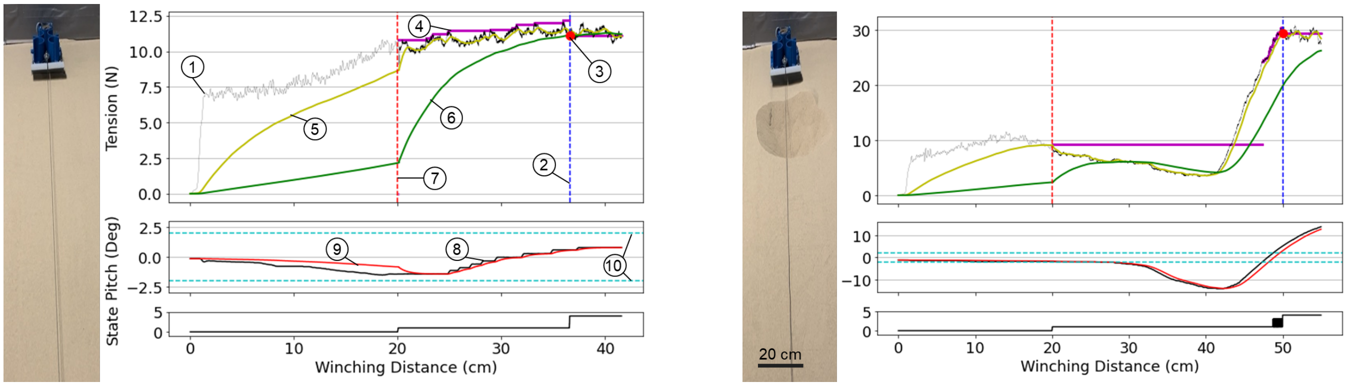

(a) Flat Terrain

(b) Hole Terrain

Fig. 8: Force-Pitch data plot of (a) flat and (b) hole terrains consist of three subplots: tension, pitch, and controller state against winching distance. Tension plot shows measured tension (1), terminal state location (2), captured force (3), recorded global max force at a position (4), smoothed tension (5), attenuated tension (6), and saturation distance location (7). The pitch plot shows measured pitch (8), smoothed pitch (9), and pitch thresholds (10).

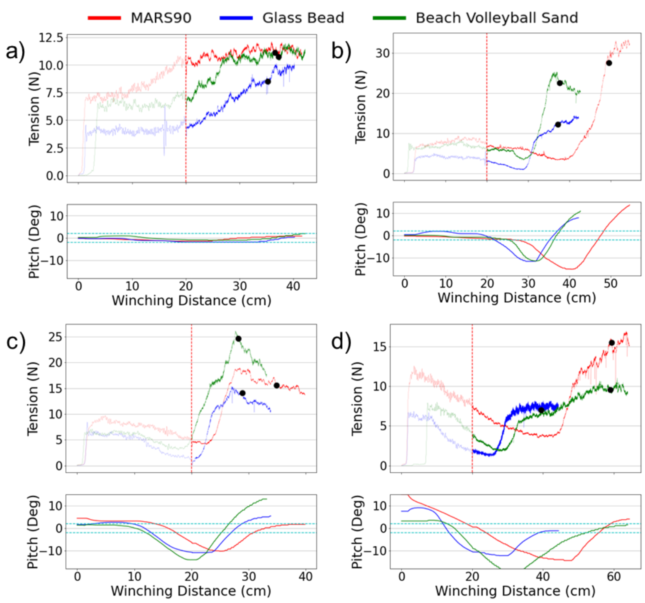

Fig. 9: Typical raw force and pitch data plots of the three granular beds by structured terrain features: (a) Flat, (b) Hole, (c) Sine, and (d) Downhill. Black dots represent the State 4 transition point.

C. Data Collection

Once the terrain features are structured, the agent is deployed at the initial position aligned straight in front of the winch module, and the tether is set to be parallel to the flat surface by adjusting the winch pulley height. We performed six trials for each media and terrain shape scenario. To observe the effectiveness of the stop condition, we continue winching for 5cm after the State 4 transition occurs. To assess the effectiveness of the stop point, we compare the force that occurs at the State 4 transition to the highest prior peak observed in the trial. Note that this is not a global comparison, which we leave to future work.

In Fig. 8 shows two example trials with the raw force data collected (1) and controller behaviors for MARS90 on two different terrain features. Fig. 8a represents the logic flow described for flat terrain (States 0 - 1 - 2 - 4). Fig. 8b shows the case (States 0 - 1 - 3 - 4) for hole terrain, which has flat, descending, and ascending terrain in series. In the tension-displacement plots, the vertical State 4 dashed line (2) and circle (3) indicate the controller terminal position and the captured tugging force, respectively. The recorded peak line (4) shows the maximum force recorded in real-time up to the winching position. We can see that this transition occurs when the smoothed (5) and attenuated (6) force lines appear horizontal for the flat case (a) while only the smoothed line is flat for the hole case (b). The d_s dashed line (7) indicates where d_s ends (at 20 cm) and State 1 is initiated.[3] The pitch, both raw (8) and smoothed (9), in Fig. 8a stay between the two horizontal dashed lines, which indicate the pitch thresholds (10). Likewise, the pitch in Fig. 8b shows both descending and ascending conditions outside of these limits. In (a), the States 0, 1 and 4 are sustained for substantial displacements, however State 2 occurs briefly between the States 1 and 4. In (b), the controller shows sustained 0 and 1 states initially followed by an oscillation between States 1 and 3 as the agent moves from descending to ascending.

V. Results

Fig. 9 illustrates the results of the agent's raw tugging force and pitch on the three granular beds and four terrains. Each type of media results in a distinct force and pitch plot, however patterns emerge when comparing these data across the different terrain features. The flat terrain (a) shows a gradual increase and saturation of the tension. The hole (b) shows consistent ascending following a descending period resulting in plateauing peaks. The sine terrain (c) looks similar to the hold in pitch, but with more pronounced peaks that diminish more rapidly. The downhill (d) shows similarities with both the hole by initially descending, but ultimately the peak appears closer to the flat condition as a mound is generated by the agent.

Fig. 10a presents distributions of the maximal forces captured by the controller (solid boxes) and the maximum force (empty boxes) recorded within the agent's travel prior

[3]By assuming $\theta_{repose} = 30°$, the approximated d_s was 24.5 cm, but we shortened it to 20 cm considering the agent workspace and granular bed sizes. We also increase the winching speed to 30 rpm (3 cm/s) rather than using the quasistatic velocity (2 mm/s) to speed up experiments within d_s.

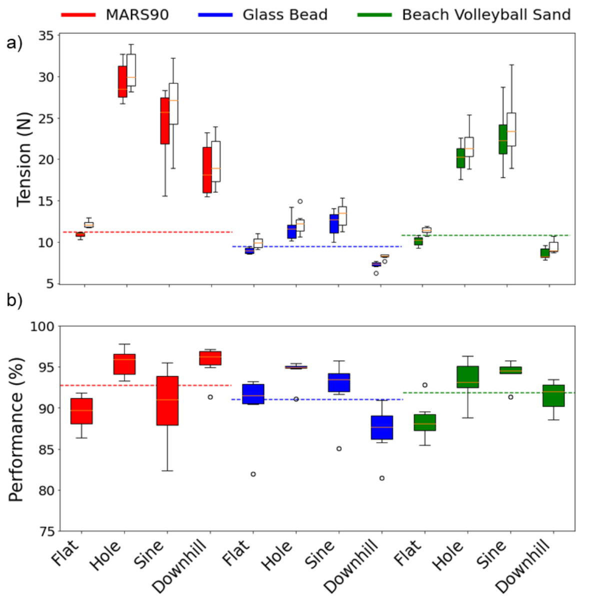

Fig. 10: The results of the controller's (a) captured force and global maximum (white box) comparison and (b) maximal force capturing performance across Granular Beds (MARS90 - red, Glass Bead - blue, Beach Volleyball Sand - green) and Terrains (in the order of Flat - Hole - Sine - Downhill)

to State 4. The dashed lines indicate the maximum of the captured forces on flat terrain trials to visually compare with other terrain features. As expected, the overall peak forces of the different media vary from one another, as the properties of the mounded material changes. Even as overall resistive forces of the media change, the hole and sine terrain shapes consistently yield the highest peak tensions within each media type. For MARS90, the hole, sine, and downhill captured force medians are 258%, 233%, and 164% of its median of the flat terrain, respectively. For Glass Bead, these medians are 123%, 142%, and 82% of its median of the flat terrain, respectively. For Beach Volleyball Sand, the medians are 199%, 218%, and 81% of the median of the flat terrain, respectively. It appears as though bumpy terrain features, but not necessarily descending slopes, present an advantage for robotic systems that use winched mounding to secure anchors that can be reliably harnessed.

Fig. 10b shows the controller's maximal force-capturing performance distributions – plotted as the ratio of the captured maximum force to the maximum observed force prior to State 4 – for each terrain feature and granular media. The dashed lines indicate the controller's average performance across all terrains, which are 92.68%, 91.02%, and 91.85% for MARS90, Glass Bead, and Beach Volleyball Sand, respectively. The mean overall performance of the controller across all conditions is 91.85%. No trial performs below 80%. This is notable since the winch is irreversible in this mechanical system, and has no information *a priori* as to which terrain class tested it will encounter.

VI. Discussion

In this work, we find that the FPGT controller logic provides near-to-peak tugging force identification on three different granular media with four different terrain features designed to challenge the controller. Not only do these trial suggest that tugging an agent to mound media can be a forceful anchoring option, but that it can be reliable across uncertain terrains. As a preliminary test of this ability to handle random terrains, we performed one trial on the unstructured sand at the Beach Volleyball Court, which was shaped from regular sports use. In this trial, the system achieved 87.5% of the observed maximum.

A. Limitations and Future Work

In this work, we limited tugging distance due to sand tank size. Therefore, we did not necessarily capture the overall global optimal characteristics of each terrain scenario. Performing long-displacement agent tugging tests would allow us to compare the controller against the best possible achievable force. However, we note that limiting overall displacement of the agent – between about 30 to 70 cm in the present study – may be desirable for certain robotic applications where tugging distance limits payload manipulation workspace. Also, because of the irreversible nature of the tugging system, an anchor that finds a conservative peak early in its movement can be reestablished again later by the winch if it were to fail during loading.

The controller introduced here for mounding anchors uses hand-tuned parameters assuming a parallel winching direction. The results cannot therefore be extrapolated to any granular media or terrain. Ultimately, these parameters could be discovered or tuned to each scenario using automated techniques with additional inputs on the robotic system. The simplicity of using only two simple sensors for the control may hold advantages, and future work could evaluate computational efficiency for potential deployment in low-power, space-restricted environments. However, future work could also explore the utility of sensor fusion with visual terrain mapping, such as with cameras, LiDAR, or orbiter imagery, to improve versatility.

VII. Conclusion

This study presents an agent winching method with a simple sensor setup – a load cell and an IMU – for maximizing lateral anchoring forces. We introduce Force-Pitch Gradient Tracking controller logic designed based on the agent tugging force model developed for plowing sand mounds. The controller performance evaluations show near-peak force capture and consistency across different granular beds and structured terrain features. These results support the potential adoption of projectile anchoring agents in future space missions on sandy terrains. For example, systems like that envisions in NASA's LCRT project, where agent anchors on the rim of a lunar crater [15] could secure distant anchor points through centralized robotic winches.

Acknowledgement

This work is funded by an Early Career Faculty grant from NASA's Space Technology Research Grants Program (#80NSSC21K0069). The authors acknowledge contributions of Angelica Pena, Laura Treers, Cyndia Cao, Amber Young, Andrew Galassi and Jungpyo Lee.

REFERENCES

[1] A. S. McEwen, E. M. Eliason, J. W. Bergstrom, N. T. Bridges, C. J. Hansen, W. A. Delamere, J. A. Grant, V. C. Gulick, K. E. Herkenhoff, L. Keszthelyi, *et al.*, "Mars reconnaissance orbiter's high resolution imaging science experiment (HiRISE)," *Journal of Geophysical Research: Planets*, vol. 112, no. E5, 2007.

[2] G. Barkó, G. Kalácska, R. Keresztes, L. Zsidai, H. Shegawu, and Á. Kalácska, "Abrasion evaluation of moon and mars simulants on rotating shaft/sealing materials: Simulants and structural materials review and selection," *Lubricants*, vol. 11, no. 8, p. 334, 2023.

[3] P. Morgan, M. Grott, B. Knapmeyer-Endrun, M. Golombek, P. Delage, P. Lognonné, S. Piqueux, I. Daubar, N. Murdoch, C. Charalambous, *et al.*, "A pre-landing assessment of regolith properties at the insight landing site," *Space Science Reviews*, vol. 214, pp. 1–47, 2018.

[4] E. F. Fukushima, N. Kitamura, and S. Hirose, "Development of tethered autonomous mobile robot systems for field works," *Advanced robotics*, vol. 15, no. 4, pp. 481–496, 2001.

[5] J. B. Matthews and I. A. Nesnas, "On the design of the axel and duaxel rovers for extreme terrain exploration," in *2012 IEEE Aerospace Conference*. IEEE, 2012, pp. 1–10.

[6] A. Stroupe, A. Huntsberger, M. Garrett, and P. Younse, "Robotic mars geology with tressa: beyond the mars rovers," in *Workshop on Robotics and Challenging Environments, ICRA*. Citeseer, 2007.

[7] B. Stenning, L. Bajin, C. Robson, V. Peretroukhin, G. R. Osinski, and T. D. Barfoot, "Towards autonomous mobile robots for the exploration of steep terrain," in *Field and Service Robotics: Results of the 9th International Conference*. Springer, 2015, pp. 33–47.

[8] P. McGarey, F. Pomerleau, and T. D. Barfoot, "System design of a tethered robotic explorer (trex) for 3d mapping of steep terrain and harsh environments," in *Field and Service Robotics: Results of the 10th International Conference*. Springer, 2016, pp. 267–281.

[9] J. J. Page, L. K. Treers, S. J. Jorgensen, R. S. Fearing, and H. S. Stuart, "The robustness of tether friction in non-idealized terrains," *IEEE Robotics and Automation Letters*, vol. 8, no. 1, pp. 424–431, 2022.

[10] T. Zhang and D. I. Goldman, "The effectiveness of resistive force theory in granular locomotion," *Physics of Fluids*, vol. 26, no. 10, 2014.

[11] L. K. Treers, C. Cao, and H. S. Stuart, "Granular resistive force theory implementation for three-dimensional trajectories," *IEEE Robotics and Automation Letters*, vol. 6, no. 2, pp. 1887–1894, 2021.

[12] T. M. Huh, C. Cao, J. Aderibigbe, D. Moon, and H. S. Stuart, "Walk-burrow-tug: Legged anchoring analysis using rft-based granular limit surfaces," *IEEE Robotics and Automation Letters*, vol. 8, no. 6, pp. 3796–3803, 2023.

[13] J. Fernandez and A. Mazumdar, "Tail-based anchoring on granular media for transporting heavy payloads," *IEEE Robotics and Automation Letters*, vol. 6, no. 2, pp. 1232–1239, 2021.

[14] K. Carpenter, S. Bandyopadhyay, H. Stuart, A. Goel, S. Moreland, C. Gebara, E. Jens, and B. Hockman, "Launchable lunar anchors," in *AIAA SCITECH 2025 Forum*, 2025, pp. 1–8.

[15] S. Bandyopadhyay, P. Mcgarey, A. Goel, R. Rafizadeh, M. Delapierre, M. Arya, J. Lazio, P. Goldsmith, N. Chahat, A. Stoica, *et al.*, "Conceptual design of the lunar crater radio telescope (lcrt) on the far side of the moon," in *2021 IEEE Aerospace Conference (50100)*. IEEE, 2021, pp. 1–25.

[16] M. Allan, U. Wong, P. M. Furlong, A. Rogg, S. McMichael, T. Welsh, I. Chen, S. Peters, B. Gerkey, M. Quigley, M. Shirley, M. Deans, H. Cannon, and T. Fong, "Planetary rover simulation for lunar exploration missions," in *2019 IEEE Aerospace Conference*, 2019, pp. 1–19.

[17] B. Percier, S. Manneville, J. N. McElwaine, S. W. Morris, and N. Taberlet, "Lift and drag forces on an inclined plow moving over a granular surface," *Physical Review E—Statistical, Nonlinear, and Soft Matter Physics*, vol. 84, no. 5, p. 051302, 2011.

[18] H. A. Oravec, V. M. Asnani, C. M. Creage, and S. J. Moreland, "Geotechnical review of existing mars soil simulants for surface mobility," in *Earth and Space 2021*, 2021, pp. 157–170.

[19] S. Kim, L. K. Treers, T. M. Huh, and H. S. Stuart, "Efficient reciprocating burrowing with anisotropic origami feet," *Frontiers in Robotics and AI*, vol. 10, p. 1214160, 2023.

[20] River Sand Inc., "Volleyball sand," 2023, accessed: 2024-09-14. [Online]. Available: https://riversandinc.com/sand/volleyball-sand/